

# Journal of Biomedical Optics

[SPIEDigitalLibrary.org/jbo](http://SPIEDigitalLibrary.org/jbo)

## **Predicting the ischemic infarct volume at the first minute after occlusion in rodent stroke model by laser speckle imaging of cerebral blood flow**

Yao Li  
Shuping Zhu  
Lu Yuan  
Hongyang Lu  
Hangdao Li  
Shanbao Tong

# Predicting the ischemic infarct volume at the first minute after occlusion in rodent stroke model by laser speckle imaging of cerebral blood flow

Yao Li,<sup>a,b</sup> Shuping Zhu,<sup>a</sup> Lu Yuan,<sup>b</sup> Hongyang Lu,<sup>b</sup> Hangdao Li,<sup>b</sup> and Shanbao Tong<sup>a,b</sup>

<sup>a</sup>Shanghai Jiao Tong University, School of Biomedical Engineering, 800 Dongchuan Road, Shanghai 200240, China

<sup>b</sup>Shanghai Jiao Tong University, Med-X Research Institute, 1954 Huashan Road, Shanghai 200030, China

**Abstract.** Stroke is a worldwide medical emergency and an important issue in stroke research is looking for the early pathophysiological markers which can predict the severity of brain injury. Decreased cerebral blood flow (CBF) has been serving as the most important indicator of ischemic stroke. Particular attention is paid to study the spatio-temporal CBF changes immediately after the onset of stroke in a rat intraluminal filament middle cerebral artery occlusion (MCAO) model and investigation of its correlation with brain infarct volume after 24 h. We implement an on-line laser speckle imaging (LSI) system, which could provide real time high spatio-temporal resolution CBF information before, during, and immediately after the rat MCAO surgery. We found a significant correlation between the affected area with 50% CBF reduction (CBF<sub>50</sub>) at the first minute after occlusion with the infarct volume. To the best of our knowledge, this is the earliest CBF marker for infarct volume prediction. Based on such a CBF–infarct volume correlation, LSI may be used as a real time guidance for improving the consistency of intraluminal filament MCAO model since the depth of filament insertion could be adjusted promptly and those unsuccessful models could be excluded in the earliest stage. © 2013 Society of Photo-Optical Instrumentation Engineers (SPIE) [DOI: 10.1117/1.JBO.18.7.076024]

Keywords: laser speckle imaging; middle cerebral artery occlusion; cerebral blood flow; infarct volume; stroke.

Paper 130092R received Feb. 17, 2013; revised manuscript received Jun. 17, 2013; accepted for publication Jun. 27, 2013; published online Jul. 25, 2013.

## 1 Introduction

Stroke is a medical emergency serving as a leading cause of morbidity and mortality worldwide and over 80% of all strokes are ischemic strokes with very limited clinical treatment options.<sup>1</sup> Intravenous tissue plasminogen activator (tPA) is the only treatment for a nonhemorrhagic stroke approved by Food and Drug Administration of the United States, which must be administered within 3 to 4.5 h of stroke onset for it to be effective in reducing the infarction volume and its functional impact.<sup>2,3</sup> An important issue in stroke research is looking for the early pathophysiological markers which can predict the severity of brain injury.<sup>4</sup> In the early hours after cerebral arterial occlusion, an initial reduction in cerebral blood flow (CBF) was first observed, which is most severe in the central perfusion territory of the artery.<sup>5</sup> Accompanying this initial prominent reduction in CBF within 1 h after occlusion, there is a decrease in cerebral metabolic rate of oxygen and an increase in oxygen extraction fraction. A series of functional and biochemical changes occurs in response to the rapid CBF reduction including a progressive reduction in protein synthesis, a disruption of normal cellular function and homeostasis, and an impaired neuronal electrical activity. With further decrease in CBF, a battery of biochemical changes occur, including declining high-energy phosphate, dropping pH, and rising lactate levels.<sup>6</sup> Brain tissues with cerebral perfusion deficits below a critical threshold experience metabolic energy failure, membrane depolarization, and subsequent

cellular swelling followed eventually by cell death. The fate of a neuron is highly dependent on the magnitude and duration of the CBF reduction.<sup>7</sup> Therefore, decreased CBF is the predominant factor associated with artery occlusion and serves as the earliest indicator of ischemia stroke.<sup>8</sup>

There have been a variety of neuroimaging methodologies for hemodynamics and metabolism of acute stroke including magnetic resonance imaging (MRI), positron emission tomography (PET), laser Doppler flowmetry (LDF), etc.<sup>9–12</sup> PET is capable of providing regional metabolism information with radiotracers employed. Using multitracer <sup>15</sup>O PET, the irreversible ischemic tissue damage area showed a very low CBF, cerebral blood volume (CBV), and metabolic rates of oxygen and glucose within 5 to 18 h after onset of stroke.<sup>9</sup> Yet, it was not able to offer diagnostic information in hyperacute stage (<3 h) due to the limitation of the methodology. MRI diffusion-weighted imaging is particularly useful in early detection of acute ischemia and can show a positive ischemic injury within minutes after stroke.<sup>10,11</sup> However, the temporal resolution is limited for MR-based study, and the accessibility for MR facilities is constrained, especially for animal studies. LDF is a widely employed technique to monitor the CBF changes in stroke animal models, which provides exquisite temporal resolution and is mostly used to offer real time CBF information during animal middle cerebral artery occlusion (MCAO) surgery.<sup>13–15</sup> However, CBF obtained by LDF is constrained to very limited locations without spatial distribution information, thus it is not able to predict the ischemia lesions precisely. The infarct volumes vary a lot even though similar CBF reductions were observed by LDF.<sup>16</sup>

Address all correspondence to: Shanbao Tong, Shanghai Jiao Tong University, Med-X Research Institute, 1954 Huashan Road, Shanghai 200030, China. Tel: +86-21-34205138; E-mail: shanbao.tong@gmail.com or Yao Li, E-mail: yaoli118@gmail.com

Therefore, it is valuable to study the changes of CBF in a high spatial and temporal resolution manner so as to find predictor of infarct volume at the earliest time point. Laser speckle imaging (LSI) technique is an optical imaging methodology which has been widely used to measure the spatio-temporal changes of blood flow. The speckle fluctuation due to blood cells motion reflects the CBF velocity, which can be measured quantitatively by laser speckle contrast analysis (LASCA).<sup>17</sup> Compared with LDF, LSI can obtain full-field CBF information with high spatial and temporal resolution. Ohshima et al.<sup>18</sup> used LSI to investigate the CBF changes during reperfusion of hypoxic-ischemic insult in immature mice and rats. They found a significant correlation between the CBF measured in the ischemic core area during the late reperfusion phase (6 and 24 h after hypoxia) and brain damage morphologically assessed by measuring the hemispheric volumes 7 days after the insult. Nevertheless, in this neonatal stroke model, the early CBF changes after occlusion were not predictive for brain damage.

In this paper, particular attention is paid to the study of spatio-temporal CBF changes in cerebral cortex immediately after the onset of stroke in a rat MCAO model. By investigating its correlation with brain infarct volume, we aimed at finding an early predictor for the ischemic infarct volume. In our approach, we implemented an on-line LSI system, which could provide real time high resolution CBF information before, during, and immediately after the rat MCAO surgery. In this study, we used intraluminal filament MCAO model to induce stroke, which is one of the most widely utilized experimental focal cerebral ischemia models for its close relevance to clinical ischemic stroke.<sup>19,20</sup>

## 2 Materials and Methods

### 2.1 Animal Preparation

Adult male Sprague-Dawley rats ( $n = 12$ ), weighing 265 to 295 g (Shanghai Slac Laboratory Animal Co., Ltd, Shanghai, China), were used in the experiments. Each animal was anesthetized with 2.5% isoflurane carrying 20% oxygen and 80% nitrogen induced through a face mask during the experiment. The rat was constrained on a stereotaxic frame and the skull was thinned to transparency by a high-speed dental drill (SDE-H37L, Marathon, Korea). Saline was used for cooling during the smoothing and glycerol was used to reduce the specular reflections and improve the optical clearing during the imaging. The protocols were approved by the Animal Care and Use Committee of Shanghai Jiao Tong University.

In order to acquire CBF image during the surgery, the rat should be placed in supine position during the surgery of the intraluminal filament MCAO model; therefore, we applied a miniature LSI (diameter: 15 mm) and fixed it on the rat skull with glass ionomer cement.<sup>21</sup> Since the head-mounted miniature imager could minimize the motion artifacts,<sup>21</sup> the surgical movements would not affect the image quality. A customized surgery board was used to adapt to this real-time LSI system. After the animal preparation, the rat was positioned on the surgery board in supine position for MCAO surgery [Fig. 1(a)].

### 2.2 MCAO Surgery

During the MCAO surgery, a midline neck incision was made and the soft tissues were pulled apart. The right common carotid

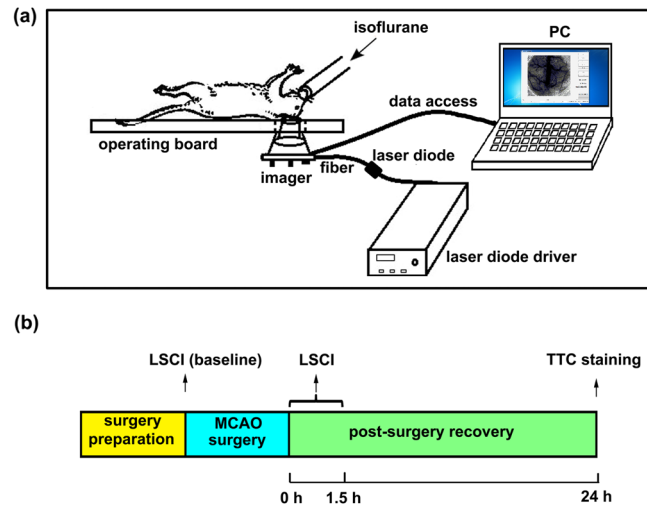


**Fig. 1** Schematic presentation of real time-laser speckle imaging system during MCAO surgery (a) and the experimental protocols (b).

artery (RCCA) and the occipital artery branch of the right external carotid artery (RECA) were dissected and ligated. The right internal carotid artery (RICA) was isolated and carefully separated from the adjacent vagus nerve. A small incision was made in the RCCA before it bifurcates to the RECA and RICA, and a monofilament nylon suture (length: 4.0 cm; diameter: 0.36 mm) with its 5-mm distal segment coated with silicone (Beijing Sunbio Biotech Co., Ltd, Beijing, China) was introduced into the RICA. The nylon suture was advanced up to 18 mm from the bifurcation of RCCA toward the right middle cerebral artery in the circle of Willis. The remaining sutures were cut and the skin was sutured.

### 2.3 Triphenyltetrazolium Chloride (TTC) Staining and Infarct Volume Calculation

The infarct volume was measured by quantitative histology using 2,3,5-triphenyltetrazolium chloride (TTC) staining technology. At 24 h after MCAO, the rat was sacrificed and the brain was removed quickly and sectioned coronally into five 3-mm thick slices. The brain slices were incubated for 20 min in 4% TTC at 37°C and then photographed. The TTC stained viable brain tissue was dark red, whereas the infarcted tissue was unstained. The slices were fixed in 4% paraformaldehyde after TTC staining. The infarct area was measured as the unstained part using ImageJ software (National Institutes of Health, Bethesda, Maryland). By subtracting the area of non-ischemic ipsilateral hemisphere from that of the contralateral side, the infarct volumes were calculated.

### 2.4 Laser Speckle Contrast Imaging

The whole experimental protocol is presented in Fig. 1(b). The raw LSI data, right before MCAO surgery, were first acquired as the baseline. In the MCAO surgery, LSIs were continuously monitored from the completion of filament insertion to 1.5 h afterwards.

A laser diode (780 nm; 10 mW; L780P010, Thorlabs, USA) powered by a driver module (LDC205C, Thorlabs, USA) was used to illuminate the rat skull with a beam expanded through a collimating lens. Raw laser speckle data (50 frames/s) were collected by a macrolens system (radius: 3.44 mm; focal length:

5.05 mm; minimum focus distance: 20 mm; custom-made to our design by GiantTec, Shanghai, China) fixed onto the printed circuit board (PCB;  $3.6 \times 3.6$  cm; Thorlabs, USA), and then imaged by a CMOS sensor ( $1024 \times 1396$  pixels; 8-bit precision; size, 2/3 in; Thorlabs, USA) on PCB. The imager was configured by software through a USB interface (pixel clock of 35 MHz, exposure time of 5 ms, area of interest of  $640 \times 640$  pixels). The exposure time of 5 ms was selected to optimize the contrast-to-noise ratio.<sup>22</sup> A custom-developed software program acquired the raw images (25 frames/stack) through a USB cable for further CBF analysis on the computer.

## 2.5 Data Processing

According to the LASCA theory,<sup>23,24</sup> blood flow velocity is related to speckle contrast value  $K$ , which is defined as the ratio of the standard deviation to the mean intensity in the speckle pattern. And  $K$  is theoretically related to the speckle correlation time  $\tau_c$  as

$$K = \left\{ \beta \left[ \frac{\tau_c}{T} + \frac{\tau_c^2}{2T^2} (e^{-2T/\tau_c} - 1) \right] \right\}^{1/2}, \quad (1)$$

where  $T$  is the camera exposure time,  $\beta$  is the coefficient inversely determined by the number of speckles in each pixel area, and  $\tau_c$  is assumed to be inversely proportional to the blood flow velocity. Therefore,  $K^2$  is inversely proportional to the blood flow velocity.

The raw speckle images were processed with temporal laser speckle contrast analysis (tLASCA) method<sup>25</sup> to obtain the contrast images of CBF with high spatial resolution. Speckle contrast value  $K_t(i, j)$  was calculated as

$$K_t(i, j) = \frac{\sigma_t(i, j)}{\langle I_t(i, j) \rangle} = \frac{\sqrt{\frac{1}{N} \sum_{l=1}^N I_{i,j,l}^2 - \left( \frac{1}{N} \sum_{l=1}^N I_{i,j,l} \right)^2}}{\frac{1}{N} \sum_{l=1}^N I_{i,j,l}}, \quad (2)$$

where  $I_{i,j,l}$  is the speckle intensity for pixel at  $(i, j)$  in the  $l$ th image frame. We used 10 frames of raw speckle images to calculate one set of speckle contrast value image, and 32 sets of contrast images were averaged out to reduce the noises. Therefore, 320 frames of raw speckle images were utilized to obtain one frame of speckle contrast value image for analysis. The acquired contrast image at the first minute after MCAO in one rat was presented in Fig. 2(a) using enhanced LASCA

(eLASCA) method<sup>26</sup> which improved the dynamic range of LASCA based on monotonic point transformation, for a more detailed visualization. Recalling that  $K_t^2$  is inversely proportional to the CBF velocity, we used the reciprocal of contrast values  $C_t = 1/K_t^2$  to calculate the relative changes in CBF velocity. In order to evaluate the CBF changes after MCAO occlusion, we normalized all the CBF images after MCAO by the baseline image pixel by pixel so as to obtain a relative CBF image defined as  $N_t(i, j, l) = C_t(i, j, l)/C_0(i, j)$ , where  $N_t(i, j, l)$  is the relative CBF velocity at pixel  $C_0(i, j)$  in the  $l$ th image frame after occlusion and  $(i, j)$  denotes CBF velocity at baseline before the surgery. Applying a threshold for relative CBF velocity as  $\epsilon$ , we may create a binary image for the  $l$ th CBF frame with pixel intensity  $B_t(i, j, l)$  defined as

$$B_t(i, j, l) = \begin{cases} 1, & \text{if } N_t(i, j, l) < \epsilon \\ 0, & \text{otherwise} \end{cases}. \quad (3)$$

One binary image calculated at the first minute after occlusion was shown in Fig. 2(b), where  $\epsilon$  was assumed equal to 50%. Such a binary evaluation could estimate the CBF reduction area more effectively, where only the pixels with a CBF level below a pre-defined threshold were shown, thus helping us to visualize and count the affected area more efficiently.

We calculated the CBF reduction area size due to occlusion by counting the number of pixels with  $B_t(i, j, l) = 1$  in the ipsilateral hemisphere and converting it proportionally to the area size in the image. In order to further demonstrate the CBF distribution within the affected area, we plotted the CBF images for the affected area in pseudocolor and overlaid it on the contrast images. The higher values in pseudocolor correspond to higher CBF velocity levels. The overlapped images were displayed in Fig. 2(c). Based on the previous studies about CBF in ischemic core<sup>27</sup> and penumbra area,<sup>28</sup> we selected two thresholds of CBF velocity reduction in this work, 25% (i.e.,  $CBF_{25}$ ) and 50% (i.e.,  $CBF_{50}$ ), respectively, to determine the affected area size.

## 2.6 Statistical Analysis

Pearson product-moment correlation coefficient analysis was performed to determine the correlation between the CBF reduction area size using thresholds of  $CBF_{25}$  and  $CBF_{50}$  during the first 90 min upon the occlusion and the infarct volume 24 h after ischemia. All data processing procedures were performed using MATLAB (Ver. 2010a, Math Works, USA).

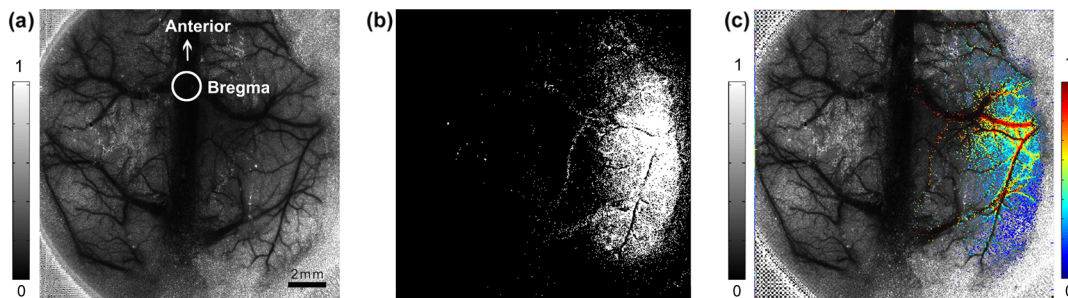


**Fig. 2** CBF reduction area computing procedures: (a) Speckle contrast image using eLASCA at the first minute after MCAO. (b) Binary image with white pixels showing a CBF velocity normalized by baseline below 50% ( $CBF_{50}$ ). (c) Overlapped images with affected area plotted in pseudocolor.

### 3 Results

#### 3.1 CBF Images with Various Levels of Infarction

The comparison of CBF images with histopathological results was shown in Fig. 3. Here, we showed two representative rats with different lesion volumes, rat one with smaller infarct volume ( $273 \text{ mm}^3$ ) in Fig. 3(a)–3(c) and rat two with larger infarct volume ( $437 \text{ mm}^3$ ) in Fig. 3(d)–3(f). The TTC staining results were shown in Fig. 3(c) and 3(f). We used the third brain section, which contained the major infarct area, for demonstration purpose. The CBF images for the  $\text{CBF}_{50}$  area in pseudocolor overlaid on the contrast images at the first minute after MCA occlusion were shown in Fig. 3(a) and 3(d). Here, the plotting followed the same style as in Fig. 2(c), where the gray color images correspond to contrast images and the images in pseudocolor show the CBF velocity information. We may see a larger  $\text{CBF}_{50}$  area in Fig. 3(d). In order to compare and visualize the CBF reduction area more clearly, we plotted the CBF image at the first minute after MCAO in pseudocolor and circled the core  $\text{CBF}_{50}$  area containing most of the  $\text{CBF}_{50}$  pixels (over 70% pixels of all). The core  $\text{CBF}_{50}$  area in Fig. 3(e) contained about  $6.8 \times 10^4$  pixels, which is much larger than the one in Fig. 3(b) with  $3.7 \times 10^4$  pixels, and this difference corresponds well with the difference in infarct volumes.

#### 3.2 Temporal Variations of CBF Reduction Area

The variations of total CBF reduction area in one rat at 1, 30, and 90 min after intraluminal filament occlusion along with the baseline image were shown in Fig. 4, for  $\text{CBF}_{25}$  [Fig. 4(a)–4(d)] and  $\text{CBF}_{50}$  [Fig. 4(e)–4(h)]. Again, the plotting follows the same way as in Fig. 2(c), where the pseudocolor images overlaying in Fig. 4(a) and 4(e) correspond to the 50% CBF reduction areas (i.e.,  $\text{CBF}_{50}$  area). It was noted that the changes of CBF reduction area over time were more prominent for  $\text{CBF}_{50}$ , and the corresponding area size increased with time.

#### 3.3 Correlation of CBF Reduction Area Size with Infarct Volume at Different Time Points

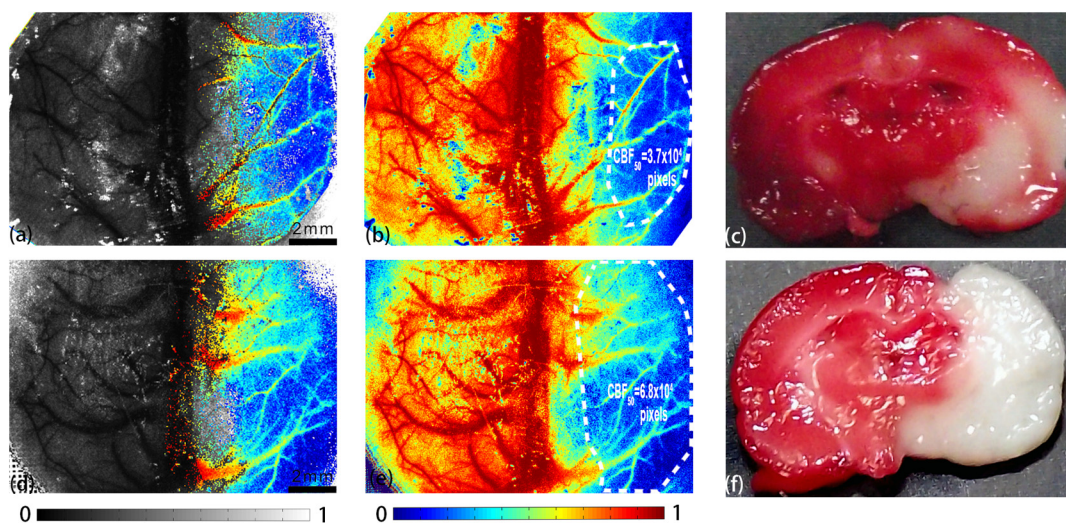
We computed the correlation coefficient  $R^2$  and  $p$  value between the relative CBF reduction area size during the first 90 min upon occlusion and the infarct volume 24 h after MCAO.

Figure 5(a) and 5(b) showed the variation of  $R^2$  using  $\text{CBF}_{25}$  and  $\text{CBF}_{50}$  methods, respectively. All data points with significant correlation ( $p < 0.05$ ) were marked out. It was clear that most of the data (73% for  $\text{CBF}_{25}$  and 93% for  $\text{CBF}_{50}$ ) in the first 30 min had correlation significance ( $p < 0.05$ ) and their correlation coefficients were higher than those within the later 60 min. Linear regression analysis indicated that CBF reduction in the early stage (within 30 min after occlusion) was predictive for the infarct volume.  $R^2$  reached the maximum at the 30th min after occlusion with  $\text{CBF}_{25}$  ( $R^2 = 0.571$ ,  $p < 0.05$ ) and at the first minute with  $\text{CBF}_{50}$  ( $R^2 = 0.540$ ,  $p < 0.05$ ). The correlations between CBF reduction area size and infarct volume for the corresponding time points were shown in Fig. 5(c) and 5(d). More interestingly, the earliest correlation happened almost immediately after occlusion in aspect of  $\text{CBF}_{50}$ , which is of great importance for prediction of infarct volume at the earliest time point and provides prompt insights for real-time surgery guidance.

### 4 Discussion

#### 4.1 CBF Changes After MCAO Surgery

In this paper, we studied the changes of CBF in the intraluminal filament MCAO surgery, especially at the early time points after occlusion of MCA. Decreased CBF serves as the earliest pathophysiological marker associated with ischemia stroke. Critical CBF thresholds below which tissues are destined to become infarcted have been examined in a variety of studies. Kohn et al. measured the CBF at 30 min and 2 h after MCA occlusion in rats by [ $^{14}\text{C}$ ] iodoantipyrine autoradiography. At 30 min after occlusion, they found about 80% of the ipsilateral hemispheric



**Fig. 3** CBF images in comparison with histopathological results for two representative rats with different lesion volumes. Here, the gray bar and color bar are similar to Fig. 2 representing the level of contrast values ( $K^2$ ) and the level of CBF (in aspect of  $1/K^2$ ). (a) CBF image at the first minute after MCAO occlusion overlaid with  $\text{CBF}_{50}$  area for rat one with smaller lesion area. (b) CBF image at the first minute after MCAO for rat one. (c) TTC stained brain section (infarct area remained white) for rat one. (d) CBF image at the first minute after MCAO occlusion overlaid with  $\text{CBF}_{50}$  area for rat two. (e) CBF image at the first minute after MCAO for rat two. (f) TTC stained brain section (infarct area remained white) for rat two. The circled area in either (b) or (e) contains the core  $\text{CBF}_{50}$ , i.e., more than 70% pixels of  $\text{CBF}_{50}$  are within this area.

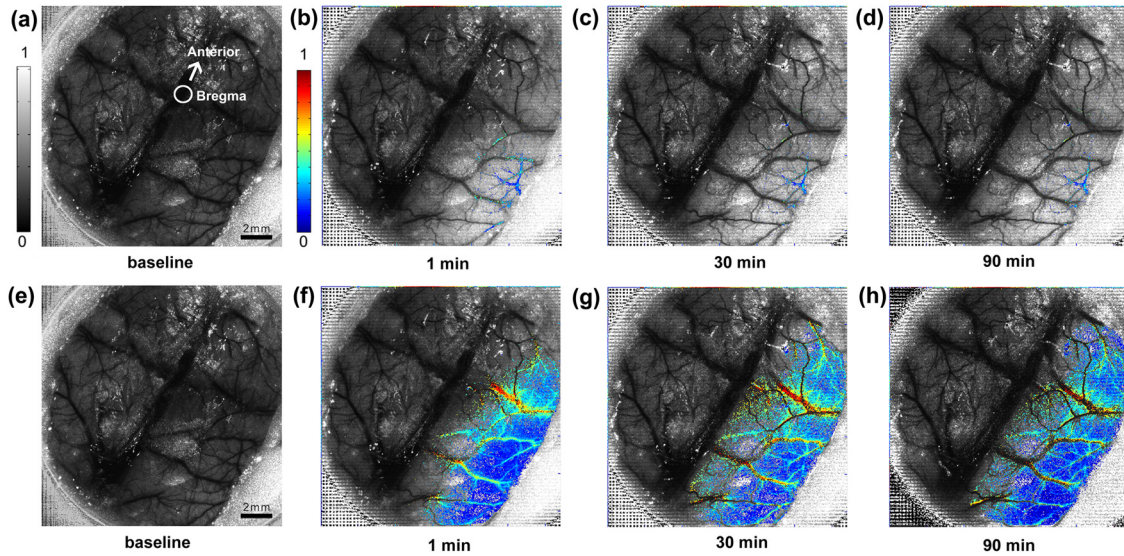


**Fig. 4** Changes of total CBF reduction area at different time points after occlusion along with baseline in one rat. (a–d) Reduction area calculated using threshold equal to 25% (CBF<sub>25</sub>). (e–h) Reduction area calculated using threshold equal to 50% (CBF<sub>50</sub>).

area exhibited CBF reductions to below 50% of the contralateral hemisphere, which remained unchanged at 2 h after occlusion.<sup>29</sup> It was further shown that tissue acidosis corresponded to a CBF value below  $0.031 \pm 0.11 \text{ mL g}^{-1} \text{ min}^{-1}$  after 2 h MCAO.<sup>30</sup> Yet, those studies relied on the autoradiographic techniques for analyzing CBF, which needed to sacrifice the animals at the time of measurement. Shen et al. used diffusion-weighted and perfusion-weighted MRI modalities to investigate cerebral ischemic injury in rats intraluminal suture MCA occlusion model.<sup>11</sup> In this way, they obtained the CBF data noninvasively

every 30 min for 3 h. The CBF threshold was derived by the correlation with TTC-infarct volume at 24 h after occlusion and was shown to be around  $0.3 \pm 0.09 \text{ mL g}^{-1} \text{ min}^{-1}$  ( $57 \pm 11\%$ ) reduction of baseline. The CBF lesion volume calculated below this threshold remained constant over time in this study.

In our work, the 50% CBF threshold also gave good correlation between CBF reduction area and TTC-infarct volume. As shown in Fig. 5(b), about 93% of the first 30 min after occlusion had significant correlation between the CBF<sub>50</sub> areas and final

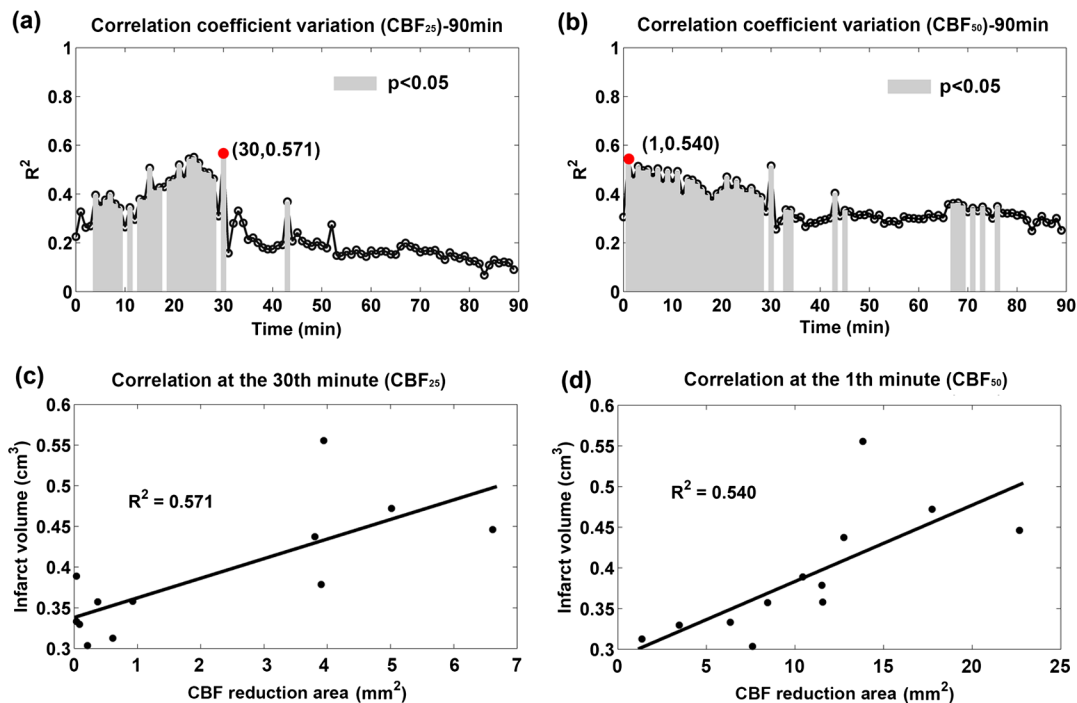


**Fig. 5** Variations of correlation coefficients between infarct volume and CBF reduction area within 90 min after occlusion using thresholds of 25% (CBF<sub>25</sub>) (a) and 50% (CBF<sub>50</sub>) (b) and the linear regression plots at their respective maximum time points (c) and (d) ( $n = 12$ ).

infarct volumes. More importantly, linear regression analysis showed that the correlation coefficient  $R^2$  reached the maximum value at the first minute after occlusion ( $R^2 = 0.54$ ,  $p < 0.05$ ). Thanks to the high spatial and temporal resolution of the CBF monitoring system, we could obtain the real time CBF data immediately after the artery occlusion and found the strongest correlation at the first minute after MCA occlusion. To the best of our knowledge, this is the earliest CBF signal for infarct volume prediction.

#### 4.2 Improving Infarct Volume Consistency by Early Brain Injury Prediction

The intraluminal filament technique has been widely used in MCAO modeling experiments for its relatively noninvasive and reversible features.<sup>19,20</sup> However, one major limitation of the intraluminal filament model is the high variability in infarct volume arising from various factors such as animal brain vascular anatomy and weight, suture material, sites of occlusion, etc.<sup>31,32</sup> The reliability and reproducibility of cerebral ischemia animal models are important in order to perform systematic study of the pathophysiology and treatment of stroke. The variability in infarct volume from animal to animal necessitates the use of large numbers of animals to discern statistical significance in experimental studies, such as therapeutic study.<sup>32,33</sup>

In the intraluminal filament MCAO model, the depth of filament insertion from the bifurcation of common carotid artery toward the middle cerebral artery should be carefully controlled to ensure a successful MCA occlusion. If the filament is advanced too much, the risks of subarachnoid hemorrhage (SAH) will increase and mortality rate of the model is high, while an insufficient filament insertion will leave the MCA unoccluded and cause a failure of modeling. In the past two decades, LDF is a widely employed technique to monitor the CBF changes during MCAO surgery to help determine whether the stroke model is successful.<sup>15</sup> To ensure a successful occlusion, a drop in blood flow velocity to 15% to 30% of baseline level on the surface of the ipsilateral dorsolateral cortex should be observed by LDF.<sup>13,34</sup> However, CBF obtained by LDF is constrained to very limited locations without spatial distribution information, thus not able to predict the infarct volume precisely. The infarct volumes vary a lot even though similar CBF reduction was observed by LDF.<sup>13-15</sup>

Our real-time CBF monitoring system can be readily used to provide full-field CBF information in a high spatio-temporal resolution during the MCAO surgery. Moreover, since we found that the CBF decreasing area immediately after MCA occlusion is closely related to the infarct volume, we may utilize it as a guidance for surgery operation to adjust the depth of filament insertion in real time so as to improve the infarct volume consistency. Also, the rats with abnormal lesions developed such as no lesions or SAH could be excluded at an early time point based on the prompt CBF prediction.

## 5 Conclusion

The goal of the work is to identify the tissue destined for infarction at the earliest time point after stroke in rat MCAO model. With our self-developed head-mounted real-time LSI system, we were able to investigate the full-field CBF changes during and after the MCAO stroke model. With special attention on the early stage (within 90 min) after MCA occlusion, we found that the CBF velocity reduction area by CBF<sub>50</sub> method at the first minute after occlusion closely correlated with the

infarct volume at 24 h after surgery. To the best of our knowledge, this is the earliest CBF signal for infarct volume prediction. Based on such a CBF–infarct volume correlation, LSI may be used as a real time guidance for improving the consistency of intraluminal filament MCAO model since the depth of filament insertion could be adjusted promptly and those unsuccessful models could be excluded in the earliest stage.

#### Acknowledgments

This work is supported by National Science Foundation of China. (Grant No. 81071192).

#### References

1. V. L. Roger et al., "Heart disease and stroke statistics—2012 update: a report from the American Heart Association," *Circulation* **125**(1), e2–e220 (2012).
2. W. Hacke et al., "Association of outcome with early stroke treatment: pooled analysis of ATLANTIS, ECASS, and NINDS rt-PA stroke trials," *Lancet* **363**(9411), 768–774 (2004).
3. E. Bluhmki et al., "Stroke treatment with alteplase given 3.0–4.5 h after onset of acute ischaemic stroke (ECASS III): additional outcomes and subgroup analysis of a randomised controlled trial," *Lancet Neurol.* **8**(12), 1095–1102 (2009).
4. R. R. Moustafa and J. C. Baron, "Pathophysiology of ischaemic stroke: insights from imaging and implications for therapy and drug discovery," *Br. J. Pharmacol.* **153**(Suppl. 1), S44–S54 (2008).
5. L. Symon et al., "Autoregulation in acute focal ischemia: an experimental study," *Stroke* **7**(6), 547–554 (1976).
6. H. A. Crockard et al., "Acute cerebral ischemia: concurrent changes in cerebral blood flow, energy metabolites, pH, and lactate measured with hydrogen clearance and 31P and 1H nuclear magnetic resonance spectroscopy. II: Changes during ischaemia," *J. Cereb. Blood Flow Metab.* **7**(6), 394–402 (1987).
7. W. D. Heiss and G. Rosner, "Functional recovery of cortical neurons as related to degree and duration of ischemia," *Ann. Neurol.* **14**(3), 294–301 (1983).
8. W. D. Heiss et al., "Progressive derangement of periinfarct viable tissue in ischemic stroke," *J. Cereb. Blood Flow Metab.* **12**(2), 193–203 (1992).
9. G. Marchal et al., "Voxel-based mapping of irreversible ischaemic damage with PET in acute stroke," *Brain* **122**(Pt 12), 2387–2400(1999).
10. N. Hjort et al., "Ischemic injury detected by diffusion imaging 11 min after stroke," *Ann. Neurol.* **58**(3), 462–465 (2005).
11. Q. Shen et al., "Pixel-by-pixel spatiotemporal progression of focal ischemia derived using quantitative perfusion and diffusion imaging," *J. Cereb. Blood Flow Metab.* **23**(12), 1479–1488 (2003), PubMed: 14663344.
12. S. Nanjundaswamy, R. A. Cohen, and M. Fisher, "Neuroimaging in acute ischemic stroke," in *Brain Imaging In Behavioral Medicine and Clinical Neuroscience*, R. A. Cohen and M. Fisher, Eds., pp. 293–308, Springer, New York, NY (2011).
13. U. Dirnagl et al., "Continuous measurement of cerebral cortical blood flow by laser-Doppler flowmetry in a rat stroke model," *J. Cereb. Blood Flow Metab.* **9**(5), 589–596 (1989).
14. N. Henninger et al., "Laser Doppler flowmetry predicts occlusion but not tPA-mediated reperfusion success after rat embolic stroke," *Exp. Neurol.* **215**(2), 290–297 (2009).
15. R. Schmid-Elsaesser et al., "A critical reevaluation of the intraluminal thread model of focal cerebral ischemia: evidence of inadvertent premature reperfusion and subarachnoid hemorrhage in rats by laser-Doppler flowmetry," *Stroke* **29**(10), 2162–2170 (1998).
16. F. Liu and L. D. McCullough, "Middle cerebral artery occlusion model in rodents: methods and potential pitfalls," *J. Biomed. Biotechnol.* Article ID 464701 (2011).
17. J. D. Briers, "Laser speckle contrast imaging for measuring blood flow," *Opt. Appl.* **37**(1/2), 139–152 (2007).
18. M. Ohshima et al., "Cerebral blood flow during reperfusion predicts later brain damage in a mouse and a rat model of neonatal hypoxic–ischemic encephalopathy," *Exp. Neurol.* **233**(1), 481–489 (2012).

19. J. Koizumi et al., "Experimental studies of ischemic brain edema. 1. A new experimental model of cerebral embolism in rats in which recirculation can be introduced in the ischemic area," *Jpn. J. Stroke* **8**(1), 1–8 (1986).
20. L. E. Zea et al., "Reversible middle cerebral artery occlusion without craniectomy in rats," *Stroke* **20**(1), 84–91 (1989).
21. P. Miao et al., "Laser speckle contrast imaging of cerebral blood flow in freely moving animals," *J. Biomed. Opt.* **16**(9), 090502 (2011).
22. S. Yuan et al., "Determination of optimal exposure time for imaging of blood flow changes with laser speckle contrast imaging," *Appl. Opt.* **44**(10), 1823–1830 (2005).
23. J. D. Briers and S. Webster, "Laser speckle contrast analysis (LASCA): a non-scanning, full-field technique for monitoring capillary blood flow," *J. Biomed. Opt.* **1**(2), 174–179 (1996).
24. D. A. Boas and A. K. Dunn, "Laser speckle contrast imaging in biomedical optics," *J. Biomed. Opt.* **15**(1), 011109 (2010).
25. H. Cheng et al., "Modified laser speckle imaging method with improved spatial resolution," *J. Biomed. Opt.* **8**(3), 559–564 (2003).
26. P. Miao et al., "Imaging the cerebral blood flow with enhanced laser speckle contrast analysis (eLASCA) by monotonic point transformation," *IEEE Trans. Biomed. Eng.* **56**(4), 1127–1133 (2009).
27. M. Lou et al., "Involvement of the mitochondrial ATP-sensitive potassium channel in the neuroprotective effect of hyperbaric oxygenation after cerebral ischemia," *Brain Res. Bull.* **69**(2), 109–116 (2006).
28. B. K. Siesjo, "Pathophysiology and treatment of focal cerebral ischemia. Part I: pathophysiology," *J. Neurosurg.* **77**(2), 169–184 (1992).
29. K. Kohno et al., "Relationship between diffusion-weighted MR images, cerebral blood flow, and energy state in experimental brain infarction," *Magn. Reson. Imag.* **13**(1), 73–80 (1995).
30. M. Hoehn-Berlage et al., "Evolution of regional changes in apparent diffusion coefficient during focal ischemia of rat brain: the relationship of quantitative diffusion NMR imaging to reduction in cerebral blood flow and metabolic disturbances," *J. Cereb. Blood Flow Metab.* **15**(6), 1002–1011 (1995).
31. Y. Kuge et al., "Nylon monofilament for intraluminal middle cerebral artery occlusion in rats," *Stroke* **26**(9), 1655–1657, discussion 1658 (1995).
32. L. Belayev et al., "Middle cerebral artery occlusion in the rat by intraluminal suture. Neurological and pathological evaluation of an improved model," *Stroke* **27**(9), 1616–1622 (1996).
33. R. J. Traystman, "Animal models of focal and global cerebral ischemia," *ILAR J.* **44**(2), 85–95 (2003).
34. J. Woitzik et al., "Comparison of different intravascular thread occlusion models for experimental stroke in rats," *J. Neurosci. Methods* **151**(2), 224–231 (2006).